Atmos. Meas. Tech. Discuss., 3, 4531–4569, 2010
www.atmos-meas-tech-discuss.net/3/4531/2010/
doi:10.5194/amtd-3-4531-2010

Atmospheric Measurement Techniques Discussions

An effective method for the detection of trace species demonstrated using the MetOp Infrared Atmospheric Sounding Interferometer

J. C. Walker, A. Dudhia, and E. Carboni

Atmospheric, Oceanic and Planetary Physics, Clarendon Laboratory, Parks Road, Oxford, OX1 3PU, UK

Received: 13 October 2010 – Accepted: 14 October 2010 – Published: 26 October 2010

Correspondence to: J. C. Walker (walker@atm.ox.ac.uk)

Published by Copernicus Publications on behalf of the European Geosciences Union.

Abstract

A detection method is demonstrated for volcanic sulphur dioxide and ammonia from agriculture using data from the MetOp Infrared Atmospheric Sounding Interferometer (IASI). The method is an extension of the Brightness Temperature Difference (BTD) technique which uses the difference in brightness temperature between a small number of channels sensitive to the target species and spectral background to determine the presence of the target species. The method described here allows instead for the use of large numbers of channels with an optimal set of linear weights which effectively suppress the spectral background allowing low-noise filters to be produced which are capable of distinguishing the target species from other parameters such as interfering species, surface and atmospheric temperature, and cloudiness without retrieving these parameters explicitly. Once generated, the filters can be applied quickly and easily to identify events of interest over a large global dataset, in near-real-time if required, and in some circumstances a degree of quantitative information can be extracted about the abundance of the target species. The theory behind the generation of the filters is first described. The filters are then used in the detection of volcanic sulphur dioxide from the eruption of the Kasatochi volcano in Alaska, beginning in August 2008, and in the detection of ammonia emissions related to agriculture over Southern Asia in May 2008. The performance of new the filters is compared against that obtained using existing filters.

1 Introduction

The IASI instrument is a Michelson-type Fourier transform spectrometer with continuous coverage in the thermal infrared from 645–2760 cm^{-1} sampled at a resolution of 0.25 cm^{-1}. The footprint of IASI consists of 4 circular IFOV's each with a radius of 12.3 km at nadir which are scanned in the direction perpendicular to the line of flight with a swath width of ~2200 km resulting in near-global coverage on a daily basis. The

AMTD
3, 4531–4569, 2010

almost total geographical coverage combined with the the large amount of spectral information means that near-real-time (NRT) processing using full retrieval schemes are not yet available for atmospheric chemistry applications. However, since detection-only algorithms do not require on-line radiative transfer calculations, they are much faster and can be used to scan the dataset quickly, for example for events of interest which may warrant further quantitative analysis, or for events which may require a rapid response for hazard avoidance. In this respect, Brightness Temperature Difference (BTD) type methods have proved very successful for the detection of trace species from infrared spectrometers and have already been used in a variety of applications including NRT volcanic plume detection.

The main difficulty in designing a trace gas detection scheme is the avoidance of false detections caused by variations in the parameters which are not measured – mainly interfering species, the temperature profile of the atmosphere, variations in surface temperature and emissivity, and the presence of cloud and aerosol. However, by using carefully selected channels these contributions can be suppressed, isolating the contribution of the target species. Existing BTD filters use only a handful of channels since the contributions of the spectral background and target species are balanced in an empirical fashion, manually selecting channels which offset the unwanted parameters. Taking the simple example of a two-channel filter, one channel is selected with a high signal due to the target species. Another channel is then selected to offset the contribution of the spectral background in the first channel whilst preserving the contribution of the target. This channel is therefore often selected in a region outside the absorption band for the target where the net contribution from unwanted parameters results in the same spectral contribution as the unwanted parameters in the target channel. A simple 50-50 difference is then taken between the observed BT in each channel to highlight the presence of the target species

$$\Delta BT = \boldsymbol{G}\boldsymbol{y} \quad (1)$$

where the weights $\boldsymbol{G}$ are given by $[1,-1]$ and the measurement vector $\boldsymbol{y} = [y_b, y_t]^T$ contains the brightness temperature in the background and target channels. In the optically

AMTD
3, 4531–4569, 2010

thin regime, this BTD is linearly related to the abundance of the target species as long as the unwanted parameters have been successfully suppressed. This method can be extended to include perhaps another one or two target or background channels, but it becomes increasingly difficult to balance the various contributions empirically without some mathematical framework for doing so. Since it is only feasible to include a few channels in this way, the hyperspectral nature of the spectrometer is not exploited effectively, and the random error associated with instrument noise in these filters remains high. In addition, there is no intrinsic way to estimate the abundance of the target. This is instead generally done a posteriori by performing full-retrievals and extracting an empirical relationship between the retrieved values and the observed BTD.

However, a great deal can be achieved with this type of filter. For example, this approach has been applied successfully for the detection of volcanic SO_2 from IASI data by using the difference between two channels in the SO_2 ν_3 vibrational band located at 1371.50 and 1371.75 cm^{-1} and two background channels at 1407.25 and 1408.75 cm^{-1} outside the SO_2 band (Clarisse et al., 2008). A similar method exists for the detection of volcanic SO_2 from the hyperspectral thermal infra-red sounder AIRS/Aura. So-called bias difference images are generated by first calculating the BTD between the observed AIRS profiles (containing the volcanic signal) and profiles generated from European Center for Medium range Weather Forecasting (ECMWF) model data, and then calculating the difference in this bias between 2 AIRS channels – one sensitive to SO2 and the other insensitive (OMI Volcanic Emissions Group TOMS, 2010). Since the presence of elevated SO_2 in the upper-troposphere is considered to be a useful marker for explosive volcanic activity and can be used as a proxy for the detection of volcanic ash which is known to pose a threat to aviation (Prata, 2009), these BTD filters have been exploited for aviation hazard avoidance. The existing four channel BTD filter for IASI data is currently used to supply an email alert to authorities within Europe who monitor the treat posed to aviation by volcanic ash clouds (Rix et al., 2009; van Geffen et al., 2009), with similar schemes in place using the AIRS/Aqua BTD filters to alert authorities in the United States (OMI Volcanic Emissions Group TOMS,

AMTD
3, 4531–4569, 2010

2010).

A BTD filter has also been used to provide the first global abundances of ammonia, which has a large contribution from agriculture with negative impacts on the environment in high concentrations. The filter uses the ammonia ν_2 band taking the BTD at 867.75 cm^{-1} and two background channels at 861.25 and 873.50 cm^{-1} (Clarisse et al., 2009). This is an example of where the BTD method is easier to implement than a full retrieval for a weakly emitting species. In this work, an estimate of global abundance of ammonia was derived using a limited number of full-retrievals to derive a scaling factor to convert the observed BTD's to estimated total column amounts of ammonia.

In this paper, an extention of the BTD method is described which allows for the generation of many channel filters with an optimal set of weights for distinguishing the target species from other contributions to the measured spectra. Once derived, the filters comprise a set of linear weights that can be applied quickly and easily by any user. However, the option to use many more channels exploits the hyperspectral nature of the spectrometer more effectively, improving signal to noise characteristics of the filters. In addition, a reasonable estimate of the abundance of the target species is provided in certain circumstances. The method outlined in this paper could in theory be used to produce trace species detection filters for other space-based spectrometers such as AIRS/Aqua, TES/Aura, or MIPAS-ENVISAT.

2 Detection method

In a given channel, the target signal is often overwhelmed by changes in the spectral background due to variations in interfering species, atmospheric temperature, surface temperature and emissivity and cloudiness. However, it is possible to remove the spectral background by computing the difference between channels sensitive to the target species and other channels with a similar contribution from the spectral background but a different target contribution. The method described here uses a similar principle of separating the target and background contributions through a linear combination of

AMTD
3, 4531–4569, 2010

channels inside and outside the target species band, but instead employs a quantitative method to generate many channel filters with an optimal set of linear weights for a more sensitive detection of the target species. The method allows the contribution of the target species to be separated from the spectral background arising from interfering species, surface properties, clouds and aerosol, and atmospheric temperature variations, without retrieving any of these other parameters explicitly.

The scheme is essentially an optimally weighted linear retrieval of the target column amount and a spectral offset. Adopting the notation in Rodgers (2000), we assume that the spectral measurements $\mathbf{y} \in \Re^m$ can be represented by the forward model F plus the total measurement error and some spectral offset

$$\boldsymbol{y} = F(x_c, \boldsymbol{u}) + \epsilon_{\text{rnd}} + \epsilon_{\text{sys}} + \text{off} \tag{2}$$

where x_c is the target gas column amount, and $\boldsymbol{u}$ represents other parameters related to the instrument, atmosphere and surface, ϵ_{rnd} is the random measurement error determined by instrument noise, and ϵ_{sys} represents systematic measurement errors due to uncertainties in parameters $\boldsymbol{u}$, and "off" is a spectral offset. Errors due to assumptions about the profile shape used to calculate the column amount x are ignored. The spectral offset can be thought of as describing uncertainties in the parameters $\boldsymbol{u}$ which correspond approximately to broadband spectral offset such as might arise from differences in the actual and modelled surface temperature, the presence of ash or ice, and the cloudiness of the atmosphere. The forward model is linearised about a climatological reference state with the expected background levels of the target gas and our best knowledge of the parameters $\boldsymbol{u}$, which should ideally reflect the particular average background conditions where the detection is applied, whereby we can write

$$\boldsymbol{y} - F(\boldsymbol{x}_0, \boldsymbol{u}) = \mathbf{K}(\boldsymbol{x} - \boldsymbol{x}_0) + \epsilon_{\text{rnd}} + \epsilon_{\text{sys}} \tag{3}$$

where the state vector is composed of the target species column amount and a brightness temperature offset $\boldsymbol{x} = [x_c, \text{off}]^T$, the linearisation point is taken to be $\boldsymbol{x}_0 = [x_0, 0]^T$ where x_0 is a climatological column amount, and the jacobian $\mathbf{K} \in \Re^{m \times 2}$ contains the elements $\mathbf{K}_{i(1,2)} = [\frac{\partial y_i}{\partial x_c}, 1]; 1 \le i \le m$ where a uniform brightness temperature perturbation

AMTD
3, 4531–4569, 2010

(1 K) is applied for all channels and y_i are in terms of brightness temperature. The retrieval of a brightness temperature offset $\hat{\text{off}}$ allows channels outside the target species band to be used as a reference point to determine x_c and acts as a sink for some error terms which may be difficult to define in advance and correspond to broadband spectral offsets. The optimal least-squares estimate $\hat{\boldsymbol{x}} = [\hat{x}_c, \hat{\text{off}}]^T$ taking into account total measurement error may then be computed as

$$\hat{\boldsymbol{x}} = \boldsymbol{x}_0 + (\mathbf{K}^T \mathbf{S}_y^{\text{tot}\,-1} \mathbf{K})^{-1} \mathbf{K}^T \mathbf{S}_y^{\text{tot}\,-1} (\boldsymbol{y} - F(\boldsymbol{x}_0, \boldsymbol{u})) \quad (4)$$

where the measurement contribution function given by

$$\boldsymbol{G} = (\mathbf{K}^T \mathbf{S}_y^{\text{tot}\,-1} \mathbf{K})^{-1} \mathbf{K}^T \mathbf{S}_y^{\text{tot}\,-1} \quad (5)$$

comprises the set of detection weights that are applied to the measured spectra to determine the presence of the target species. The total column amount given by $\hat{x}_c$ is not intended to be an accurate retrieval of the target species but rather simply a metric for determining whether levels of the gas are enhanced with respect to the climatological background. The actual value of the measured column amount depends on the assumed altitude distribution of the model plume, the altitude of the plume in the real atmosphere, whether or not the weak absorption limit applies whereby radiative transfer can be assumed to be linear, the conditions of thermal contrast with the surface where this is visible, and how effectively the spectral background has been suppressed. In the rest of this paper, the units that are adopted to described the apparent column amount determined from Eq. (4) are Estimated Dobson Units (EDU) to emphasize that these do not necessarily give an accurate idea of the true column amount.

The matrix $\mathbf{S}_y^{\text{tot}} \in \Re^{m \times m}$ is the total measurement error variance-covariance which should ideally approximate the "true" total error variance-covariance $(\epsilon^{\text{rnd}} + \epsilon^{\text{sys}})(\epsilon^{\text{rnd}} + \epsilon^{\text{sys}})^T$ for the atmospheric conditions where the detection is applied with background levels of the target gas. The use of the total measurement error variance-covariance as a weight matrix for the least squares minimisation in Eq. (4) differs from the commonly adopted inversion process, which for reasons of computational efficiency tends

AMTD
3, 4531–4569, 2010

to use only the random error variance-covariance to weight measurements, computing the systematic error contribution a posteriori if small enough to be ignored, or else retrieving other parameters either beforehand, or jointly with the target gas. It can be shown that the use of the total error to weight the measurements in a least squares estimation of the target parameter is equivalent to a joint retreival of the target together with all parameters contributing to the systematic error including their respective uncertainties as a prior constraint (von Clarmann et al., 2001). If the total measurement error variance-covariance matrix $\mathbf{S}_y^{\text{tot}}$ in Eq. (4) is widely correlated, the contribution of the systematic errors in $\hat{\boldsymbol{x}}$ is almost entirely suppressed as long as there is sufficient spectral information about all parameters, the errors are close to Gaussian and linear. By inverting the measurements in this way, the target species can be identified and separated from the contribution of other unwanted parameters.

In this paper, the $\mathbf{S}_y^{\text{tot}}$ matrix is computed either by modelling errors using appropriate perturbations to the various physical parameters involved within the forward model, or by using an ensemble of spectra to compute the variance-covariance of a large number of measured spectra with background levels of the target gas representative of the given atmospheric conditions.

2.0.1 Modelling method

The first approach, which does not rely on samples of measured spectra, involves the construction of $\mathbf{S}_y^{\text{tot}}$ considering simple perturbations to appropriate parameters within the forward model such as interfering species, atmospheric temperature, surface temperature, and cloudiness, which can then be combined with the random error determined from instrument noise to calculate an approximation of the true total error variance-covariance denoted $\mathbf{S}_y^{\text{mod}}$

$$\mathbf{S}_y^{\text{tot}} = \mathbf{S}_y^{\text{rnd}} + \mathbf{S}_y^{\text{sys}} \tag{6}$$

AMTD
3, 4531–4569, 2010

$$\approx \mathbf{S}_y^{\mathrm{rnd}} + \sum_{i=1}^{N} \mathbf{K}_i \mathbf{B}_i \mathbf{K}_i^T = \mathbf{S}_y^{\mathrm{mod}} \quad (7)$$

where $\mathbf{S}_y^{\mathrm{rnd}}$ is the random measurement error variance-covariance determined by instrument noise and $\mathbf{S}_y^{\mathrm{sys}}$ is the systematic component of measurement error. The systematic component of measurement error is computed in general by considering the combination of N error sources which are assumed to be independent. In general, for each error source, $\mathbf{S}_y^{\mathrm{sys}}$ is computed considering the $p \times p$ error variance-covariance matrix $\mathbf{B}_i$ and the corresponding jacobian $\mathbf{K}_i \in \Re^{m \times p}$. The error variance-covariance matrix $\mathbf{B}_i$ could for example represent the 1σ climatological variability in a p-level profile of water vapour in which case $\mathbf{K}_i \in \Re^{m \times p}$ is computed for the p profile levels such that the jacobian contains the elements $\mathbf{K}_{\mathrm{jk}} = \frac{\partial y_j}{\partial \mathrm{H2O}_k}$. The systematic component of measurement error could on the other hand include simply a column perturbation to an interfering species, or a perturbation to surface temperature, or a perturbation due to the presence of cloud, depending on how much detail is included in the construction of the $\mathbf{S}_y^{\mathrm{tot}}$ matrix.

Although ideally the modelled spectrum $F(\boldsymbol{x}_0, \boldsymbol{u})$ about which the jacobian $\mathbf{K}_{i(1,2)} = [\frac{\partial y_i}{\partial x_c}, 1]; 1 \le i \le m$ is calculated should be equivalent to the expected mean spectrum $\bar{\boldsymbol{y}}$ for the atmosphere with background levels of the target gas with mean concentrations of interfering species, mean conditions of cloudiness, surface temperature etc., in practice this is difficult to achieve due difficulties in defining and modelling the mean atmospheric conditions. The errors are instead calculated around the assumed linearisation point $[\boldsymbol{x}_0, \boldsymbol{u}]$ which is chosen for convenience to represent clear-sky conditions, assuming that cloudiness, as well as other broadband features such as surface temperature changes, can be accounted for by retrieving the target jointly with a spectral offset.

AMTD
3, 4531–4569, 2010

2.0.2 Ensemble method

Using the second so-called ensemble approach, $\mathbf{S}_y^{\text{tot}}$ is computed considering an appropriate ensemble of N measured spectra to construct an estimate of the total measurement error variance-covariance denoted $\mathbf{S}_y^{\text{obs}}$

$$\mathbf{S}_y^{\text{tot}} \approx \mathbf{S}_y^{\text{obs}} = \frac{1}{N}\sum_{i=1}^{N}(\boldsymbol{y}_i - \bar{\boldsymbol{y}})(\boldsymbol{y}_i - \bar{\boldsymbol{y}})^T \tag{8}$$

where $\bar{\boldsymbol{y}}$ is the calculated mean spectrum for the ensemble

$$\bar{\boldsymbol{y}} = \frac{1}{N}\sum_{i=1}^{N}\boldsymbol{y}_i \tag{9}$$

However, this approach depends on the availability of an appropriate ensemble of spectra where there is some confidence that the levels of the target species are not enhanced. When the source of the gas is well defined, as for volcanic SO_2 in the free troposphere, the selection of an appropriate ensemble with background levels of the target species can be performed relatively easily. In the case where spectra which do contain enhancements are mistakenly included in the ensemble, this acts to reduce the sensitivity of the filter to the target species, and for gases with more diffuse sources of enhancements, e.g., ammonia, finding appropriate spectra without enhancements can be more challenging. The mean spectrum $\bar{\boldsymbol{y}}$ calculated in Eq. (8) should be the equivalent to the modelled spectrum $F(\boldsymbol{x}_0, \boldsymbol{u})$ in Eq. (4) about which the jacobians $\mathbf{K}_{i(1,2)} = [\frac{\partial y_i}{\partial x_c}, 1]; 1 \le i \le m$ are calculated. However, as mentioned previously, in practice this is difficult to achieve due to problems defining and modelling the mean atmospheric conditions. So that the choice of the linearisation point is consistent with the calculation of the total error $\mathbf{S}_y^{\text{obs}}$ in Eq. (8), $\bar{\boldsymbol{y}}$ should be used in place of $F(\boldsymbol{x}_0, \boldsymbol{u})$ in Eq. (4) when using this method, which ensures that the climatological value of the target species x_c is retrieved when levels of the target species are not enhanced over

AMTD
3, 4531–4569, 2010

those represented by the mean background spectrum $\bar{\boldsymbol{y}}$. Using this method there is much less need for the inclusion of the brightness temperature offset and in fact this can usually be omitted in this case.

2.0.3 Channel selection

The success of the filter mainly depends on the construction of the $\mathbf{S}_y^{\mathrm{tot}}$ matrix and how closely this represents the true total measurement error variance-covariance of the background atmosphere, and a careful selection of channels using quantitative methods is not generally necessary. In most cases, the problem of which channels to use can be solved by a careful qualitative selection of a suitable block of channels. The main factors to be considered are that the chosen region should have a relatively strong signal from the target species and should ideally also include regions with little or no contribution from the target to maximise the available contrast with the spectral background. Evidently, spectral regions which cannot be modelled adequately should be avoided where possible.

In many cases, most channels will be highly correlated with a significant number of other channels and the correlations in $\mathbf{S}_y^{\mathrm{sys}}$ will successfully suppress the systematic error terms, as long as these errors are a good enough approximation of the true measurement error covariance, and a large enough number of channels have been included to ensure that there is adequate information about all parameters. Therefore, the problem of trying to avoid or minimise the contribution of systematic errors only arises in cases where some of these errors are uncorrelated with the errors in other channels, or when the number of channels used is very small. In these cases, it may be necessary to perform a quantitative channel selection to ensure that uncorrelated systematic errors are avoided as far as possible, or in cases where only a small number of channels are used, to ensure that an optimised set of channels are included for detection of the target species which minimise both the random and systematic errors incurred. This may be achieved by examining the information content of the filter with respect to the target species as more channels are added.

AMTD
3, 4531–4569, 2010

Since $\mathbf{S}_y^{\text{tot}}$ is in general widely correlated, the only way to ensure that the best combination of channels has been selected would be to test every permuation of k out of I channels. However, since testing every possible combination of even a relatively small set of channels is computationally unfeasible, a sequential approach to the addition of new channels is adopted as a compromise. The first step involves finding the top two channels in the chosen region with the lowest retrieval error σ_c^2 for the target component, i.e., the SO_2 column amount, by searching through all permutations of channel pairs propagating the total measurement error through the retrieval according to

$$\mathbf{S}_x^{\text{tot}} = (\mathbf{K}^T \mathbf{S}_y^{\text{tot}^{-1}} \mathbf{K})^{-1} \tag{10}$$

where $\mathbf{S}_x^{\text{tot}}$ is the retrieval error variance-covariance for the target column amount and spectral offset $\hat{\boldsymbol{x}} = [\hat{x}_c, \hat{\text{off}}]$ and $\mathbf{K}$ is the corresponding jacobian. The top pair of channels with the lowest target retrieval error σ_c^2 is then assessed in combination with each remaining channel. Each successive combination must generally be evaluated globally so that the search for the 3rd channel involves $I-2$ inversions of a 3×3 $\mathbf{S}_y^{\text{tot}}$ matrix and so on, and hence the search becomes progressively slower as more channels are added. Since $\mathbf{S}_y^{\text{tot}}$ is generally non-sparse, it is not possible to break the problem down into a series of smaller inversions as would be possible with a diagonal or block diagonal $\mathbf{S}_y^{\text{tot}}$ without losing information about the spectral correlations. The best combination of $k+1$ channels may then be assessed by computing the information content H in bits obtained about the target parameter by including the additional channel

$$H = -\frac{1}{2}\log_2\left(\frac{(\sigma_c^2)_{k+1}}{(\sigma_c^2)_k}\right) \tag{11}$$

where $(\sigma_c^2)_k$ is the target retrieval variance computed for k channels and $(\sigma_c^2)_{k+1}$ is the target retrieval variance computed for $k+1$ channels. Channels may be added in this way until the inclusion of an additional channel results in a negligible information gain or reduces the information content of the filter on the target parameter.

AMTD
3, 4531–4569, 2010

2.0.4 Detection threshold

Once a suitable set of channels have been defined, the apparent target column amount given in Eq. (4) may be compared against a threshold which indicates a positive detection with a certain confidence. An approximate estimate of the level of confidence for a particular detection can be gauged by comparison of the enhancement, $\hat{x}_c - x_0$, against the total error standard deviation σ_c^{tot} for the target gas column. The target total error variance $\sigma_c^{tot^2}$ is the target component of

$$\mathbf{S}_x^{tot} = (\mathbf{K}^T \mathbf{S}_y^{tot^{-1}} \mathbf{K})^{-1} \tag{12}$$

From Eq. (4), it can be seen that the difference between the detected column and the climatological column corresponds to the target component of $\boldsymbol{Gy} - x_0$ in the absence of biases. Hence, we can calculate

$$Z = \frac{\boldsymbol{G}\mathbf{y} - x_0}{\sigma_c^{tot}} \tag{13}$$

where σ_c^{tot} is expressed in the same units as the apparent column amount. Depending on the application a suitable Z-number can be defined for a positive detection

$$\hat{x}_c > x_0 + Z\sigma_c^{tot} \tag{14}$$

The estimate of the detection threshold should be treated cautiously, however, since in some cases the sources of error may not be Gaussian or linear, and there may be long tails associated with the true distributions.

2.1 Case study 1: Volcanic emissions

The detection method is tested for SO_2 from the eruption of the Kasatochi Volcano in the Aleucian Islands, Alaska, in early August 2008. All spectral modelling was performed using the Reference Forward Model (RFM). Details about the RFM can be

AMTD
3, 4531–4569, 2010

found in the online manual (Dudhia, 2008). An an appropriate viewing angle correction was applied to the measured spectra before application of the filters.

Ordinarily, SO_2 is concentrated in the boundary layer with total column amounts of less than 0.1 DU. Sources of SO_2 contributing to background levels in the lower troposphere include the slow degassing from volcanoes, burning of fossil fuels and biomass, and tin smelting. Figure 1 shows the spectral contribution of climatological concentrations of SO_2. There are two emission features in the thermal infra-red: the symmetric stretch ν_1 band centred on 1152 cm^{-1} and the antisymmetric stretch ν_3 band centred on 1362 cm^{-1}. The nominal NEΔT at 280 K between 1000–1200 cm^{-1} ranges between 0.950 and 0.165 K and the NEΔT at 280 K between 1300–1410 cm^{-1} ranges between 0.980 and 0.105 K (Cayla et al., 1995). Therefore, the signal from typical background levels of SO_2 are well below the noise level of the instrument. Absorption in the ν_1 band is not as strong as absorption in the ν_3 band. However, the atmosphere is more transparent in the region of the ν_1 band. The ν_3 feature, on the other hand, is obscured by strong water vapour absorption, and so SO_2 can in general only be sensed in this region at higher altitudes.

The eruption of Kasatochi beginning on 7 August 2008 caused significant disruption to air-traffic due to the volcanic ash emitted (Guffanti et al., 2008). On 8 August, a plume of ash and SO_2 was observed at an estimated altitude of 12.5 ± 4 km, with total column amounts of SO_2 estimated at 311 DU on the first day corresponding to BTD's of up to 36 K using the four channel filter (Karagulian et al., 2010). Two days later the plume had spread southward into the Pacific and OMI/Aura measured maximum column amounts of 105 DU (OMI/Aura [Internet], 2010). Figure 2 shows examples of spectra acquired inside and outside of the volcanic plume on this date. The IASI instrument is easily sensitive enough to detect the very large signal due to SO_2 within the plume. However, the challenge in designing detection filters is to make them as insensitive as possible to unwanted parameters such as clouds and water vapour, which have a large spectral contribution and are highly variable. Therefore, for each filter we also examine the distribution of values in a region of atmosphere outside the plume to examine how well

AMTD
3, 4531–4569, 2010

these other parameters have been suppressed. If these other parameters have been suppressed successfully, we expect the climatological total column amount of SO_2 to be recovered (=0.076 DU) in these cases using the new method.

The results using the existing four channel filter are shown in Fig. 3 for the evening of 10 August 2008 where the maximum BTD is around 6 K. The variation in the background values in a selected region outside of the plume normalised with respect to the maximum BTD observed inside the plume are also shown. As can be seen in Fig. 3, the filter performs very well and the variation in the spectral background is generally less than 1% of the maximum value in the plume. These results are now compared against the results obtained using new filters for SO_2.

2.1.1 ν_1 band filter

An SO_2 filter was constructed using all channels between 1000–1200 cm^{-1} in the vacinity of the ν_1 band. Checking the information content of the filter using the approach described in Sect. 2.0.3 indicates that all channels in this region contribute at least some information about the target species and none of the channels in this region have a negative impact on information content. Therefore, it is convenient to simply use the entire measurement block to generate the filter. Note that using this method purely background channels with no SO_2 signal can also contribute information about SO_2 since they help to define the spectral baseline against which SO_2 is determined. The region around the SO_2 ν_1 band is optically thin provided that the atmosphere is clear of ash and cloud, with sensitivity to the surface and boundary layer. The region avoids an ice signature present mainly between 800–1000 cm^{-1}. However, the region overlaps strong reflections from the quartz Reststrahlung band between 1100–1250 cm^{-1} (Ed. Pavelin, Met. Office, personal communication) which have much sharper spectral dependencies, which cannot at present be modelled using the RFM, and restrict the use of the filter over some land surfaces in arid regions. Two approaches are considered for the construction of the SO_2 filter using the ν_1 band:

AMTD
3, 4531–4569, 2010

1. The $\mathbf{S}_y^{\text{tot}}$ matrix in Eq. (4) is constructed using the modelling approach ($\mathbf{S}_y^{\text{tot}} \approx \mathbf{S}_y^{\text{mod}}$) as in Eq. (7) considering simple perturbations to forward model parameters. Climatological 1σ column perturbations are applied to interfering species with variability above the level of instrument noise (mainly ozone and H_2O) using the profile uncertainties defined for the mid-latitude atmosphere in the IG2 climatological database (Remedios et al., 2007), which is also used as the linearisation point $[\boldsymbol{x}_0, \boldsymbol{u}]$. A 20 K perturbation is applied to surface temperature, and variability due to cloudiness is modelled using 15 independent homogenous optically thick cloud layers at 1 km intervals from 1–15 km. Each error source is assumed to be independent of the others.

2. The $\mathbf{S}_y^{\text{tot}}$ matrix is constructed using the ensemble approach ($\mathbf{S}_y^{\text{tot}} \approx \mathbf{S}_y^{\text{obs}}$) as in Eq. (8) using an ensemble of 2253 measured spectra in a region without SO_2 enhancements in the box bounded by the [lat,lon] coordinates [32,45] and [−150, −135] on the 10 August 2008 to construct an estimate of the true total error measurement variance-covariance matrix for the background atmosphere in the vicinity of the volcanic plume.

Figure 4 shows the SO_2 detected using the ν_1 band filter where $\mathbf{S}_y^{\text{tot}}$ is constructed using the methodology described in Case (1) using the modelling approach. The plume of SO_2 is clearly visible in the Pacific Ocean. The shape of the plume appears broadly similar to that observed using the four-channel filter in Fig. 3 (which uses the ν_3 band rather than ν_1 band absorption). However, the extent of plume appears to be more restricted in this case. Absorption in the ν_1 band is not as strong as for the ν_3 band feature. However, the atmosphere is more transparent in the region of the ν_1 band, except in the presence of ash, whereas in the region of the ν_3 band feature there is very strong overlapping absorption due to water vapour. It is likely that the apparent reduced geographical extent of the plume as observed using the ν_1 band filter is due to reduced sensitivity of the ν_1 band compared to the ν_3 band at higher altitudes for SO_2 observed above the dense volcanic ash layer that was present in this plume. The

AMTD
3, 4531–4569, 2010

normalised variation in the background within the box shown in Fig. 4 does not show any obvious structure and the values appear to be normally distributed which indicates that the variations in the spectral background due to parameters such as ozone and cloudiness have been effectively suppressed. There is a very slight negative offset in the distribution of the values which in the normalised fractional units is reported as −0.000194 rather than the expected 0.00230 (=0.076 DU) if the expected climatological amount of SO_2 were to be retrieved. The reported 1σ variation for this filter is 0.0022 (=0.734 EDU) which is slightly less than the observed RMS of the background field of 0.0055.

The detection of SO_2 using the ν_1 band where $\mathbf{S}_y^{\text{tot}}$ is constructed using the ensemble approach explained in Case (2) is shown in Fig. 5. Since the background values shown in the figure were used as the ensemble to generate the filter, this represents the ideal case of what can be achieved in terms of suppression of the spectral background. The reported 1σ sensitivity of 0.0024 (0.812 EDU) of the filter matches the observed RMS of the background which was computed as 0.0024, and the mean value of the background observations yields the expected climatological value of SO_2, as expected. It is assumed that the weights calculated using this ensemble are representative of a wider area including the plume and surrounding background observations. In theory, it should be possible to use a more general ensemble of spectra e.g., selected over a carefully chosen region in a given season to generate climatological estimates of $\mathbf{S}_y^{\text{tot}}$ that are optimised to detect enhancements for a given time of year and location.

2.1.2 ν_3 band

The ν_3 band filter uses all channels between 1300–1410 cm^{-1}. The ν_3 band is generally more sensitive to SO_2 than the ν_1 band, except in the boundary layer, which is mostly obscured by interference from optically thick water vapour lines in this case. Since there are no sharp emission features not modelled by the RFM and the surface cannot be seen, there are no restrictions on surface type. However, as can be seen in Fig. 2, the ν_3 band filter sits on the edge of the water vapour band, and is therefore

AMTD
3, 4531–4569, 2010

sensitive to variability throughout the troposphere. For this reason, $\mathbf{S}_y^{tot}$ is more difficult to parameterise using the modelling approach. The main problem is variability due to water vapour itself since this accounts for over two orders of magnitude more variance than the other parameters. Three approaches are therefore considered which mainly differ in their treatment of water vapour:

1. $\mathbf{S}_y^{tot}$ is constructed considering a 1σ column perturbation to the temperature and water vapour profile as defined for the mid-latitude atmosphere in the IG2 climatological database (Remedios et al., 2007), a 20 K perturbation is applied to surface temperature and perturbations representing 15 independent homogenous optically thick cloud layers at 1 km intervals from 1–15 km are included.

2. As in (1) but now $\mathbf{S}_y^{tot}$ is constructed considering a **B** matrix for water vapour on 27 levels corresponding the a standard variance-covariance used in the Met Office NWP SAF 1D-Var scheme and similarly temperature is modelled considering a **B** matrix on 44 levels.

3. The $\mathbf{S}_y^{tot}$ matrix is constructed using an ensemble of 2253 measured spectra in a region without SO_2 enhancements in the box bounded by the [lat,lon] coordinates [32, 45] and [−150, −135] on the 10th August 2008 to construct an estimate of the true total error measurement variance-covariance matrix for the background atmosphere in the vicinity of the eruption.

Figure 6 shows the results obtained for Case (1) described above whereby water vapour variability is modelled considering a 1σ column perturbation. Although the variation in the background without SO_2 enhancements is mostly less than 1%, there are some clear systematic drifts in the retrieved background. Firstly, the mean value of the background is higher than the expected climatological background with a positive offset of 0.0064 rather than the expected 0.0022 in fractional units. In addition the values vary periodically. These variations are associated with the sideways viewing function of the instrument. In the case of sensitivity to different levels in the troposphere, a simple viewing angle correction applied to the measured spectra cannot fully correct for

AMTD
3, 4531–4569, 2010

changes in observed radiance with satellite zenith angle. There are also other drifts in the background values not associated with the sideways viewing function of the instrument. Upon inspection it was found that these drifts in the background correspond to gaps between clouds, where the measurements are sensitive to water vapour throughout the troposphere. It is likely that in this case a column perturbation of water vapour is not a good enough representation of the variability. Instead, therefore, in Case (2) a perturbation is applied to water vapour considering a **B** matrix with more realistic correlations between vertical levels. In this case, the systematic drifts in the background appear to be somewhat improved over Case (1) as can be seen from Fig. 7.

However, the best results are obtained using the ensemble method described in Case (3) shown in Fig. 8. Since both nadir viewing and sideways viewing measurements are used in the ensemble, the periodicity in the background values associated with the sideways scanning of the instrument is now also suppressed, and other drifts associated with the inadequate representation of the vertical variability in the troposphere in the modelling approach have now also disappeared. Here, the distribution of the background values is normally distributed around a typical climatological value of the SO_2 column. Using this filter, the variations in the background values are mostly below 0.1% of the maximum apparent column amount in the plume. This is around an order of magnitude more sensitive than both the ν_1 band and four channel filters.

2.2 Case study 2: Emissions from agriculture

The first global distributions of tropospheric ammonia were derived using the ν_2 vibrational band taking the BTD at 867.75 cm^{-1} and two background channels at 861.25 and 873.50 cm^{-1} (Clarisse et al., 2009) . The gas is present mainly in the boundary layer with very low concentrations higher in the troposphere. It is converted to ammonium sulphate and ammonium nitrate on the time-scale of days which then play a role in the long-range transport of acidic pollutants. We focus on a region of Southern Asia identified by Clarisse et al. (2009) as an area containing strong sources of ammonia from agriculture and compare the results obtained using the three channel filter against

AMTD
3, 4531–4569, 2010

results obtained using the new filter.

The new detection filter for ammonia was created using the ν_2 band centred on 950 cm^{-1} including all channels between 800 and 1000 cm^{-1} using the modelling method to construct $\mathbf{S}_y^{tot}$. As can be seen from Fig. 9, this region is optically thin in the absence of cloud. In these cases, characterising atmospheric variability using the modelling approach tends to be relatively straightforwards. The ensemble method, on the other hand, is more difficult to apply in this case due to the more diffuse distribution of detectable ammonia in the atmosphere. Figure 9 shows the spectral contribution of climatological concentrations of ammonia as defined in the IG2 climatology mid-latitude atmosphere. The nominal NEΔT at 280 K between 800–900 cm^{-1} is between 0.145–0.150 K (Cayla et al., 1995), and so according to Fig. 9 background concentrations of ammonia such as are observed in non-polluted regions or over ocean are expected to be well below the noise level of the instrument.

To construct $\mathbf{S}_y^{tot}$, variability due to interfering species was modelled considering 1σ total column perturbations to water vapour, ozone, and carbon dioxide as defined in the mid-latitude IG2 climatology which was also used as the linearisation point. Variability due to atmospheric temperature was modelled considering a 1σ column perturbation. Surface temperature and emissivity variability (assuming no spectral dependence) was modelled considering a 20 K perturbation and zero thermal contrast was assumed with the first atmospheric layer. Cloudiness was modelled considering 15 independent optically thick cloud layers in the troposphere between 1 and 15 km.

The ammonia filters were applied across a region of Asia in an area with persistent, high concentrations of ammonia due to intensive agricultural practices, as identified by Clarisse et al. (2009). Cloudy pixels were removed using the method by Hadji-Lazaro et al. (2001) to ensure that any areas of high ammonia which may have appeared low due to being hidden by cloud were not included. Figures 10 and 11 show ammonia as seen by the 3 channel filter and new filter respectively for the morning overpass on the 13 May 2008. An estimated total column amount has also been derived in this case for the 3 channel ammonia filter. This estimate was derived by

AMTD
3, 4531–4569, 2010

calculating a set of weights for the 3 channels using the same methodology as for the many channel filter, rather than using the simple 50-50 weighting between target and background channels. Error analyses performed for the new filter and three channel filter indicate that the detection error for the new filter is improved by over a factor 8 in comparison to the three channel filter, mainly due to the reduction in random noise. This implies that the sensitivity achieved by the many channel filter corresponds to averaging more than 64 orbits using the existing filter. The number of positive detections in the 99% confidence interval (Z-value = 2.725) was much higher for the new filter. Figure 12 shows a map of landuse derived from the FAOSTAT database for the year 2008 (Food and Agriculture Organization of the United Nations, 2008) overlaid with the ammonia field generated by the new filter to highlight the correspondence between areas of high ammonia and intensively farmed regions. Particularly high amounts of ammonia are found over an intensively cultivated region of India and Pakistan known as Indo-Gangetic Plane. In Fig. 10, the three channel filter picks out the strongest areas of emission across the Indo-Gangetic Plane, as well as some areas of high ammonia further north. However, much more detail is visible using the new filter along the Indo-Gangetic Plane in Fig. 11, with areas of high ammonia further south across India and transport out into the Indian Ocean also visible. There also appears to be a sharp boundary corresponding to the beginning of the Himalaya mountains where ammonia concentrations are expected to be lower. Using the new filter, individual areas of agricultural production can be discerned further north with an area of high ammonia in the Fergana Valley near Tashkent, in Uzbekistan (in the area around 41° N 74° E), which was identified as a strong source by Clarisse et al. (2009) in their yearly averaged ammonia emissions for 2008, attributed to the pooling of agricultural emissions in stangnant air. Also visible are areas of high ammonia further to the north and east, north of Tian Shan Mountain Range, Dzungaria, which were also identified as ammonia hotspots. In Fig. 12, these areas can be seen to correspond to intensively farmed regions. Tests performed on the ammonia filter using RTTOV simulated IASI spectra for a range of desert surfaces with realistic emissivities (Ed Pavelin, Met Office, personal

AMTD
3, 4531–4569, 2010

communication), did not indicate indicate any false detections over arid regions, and so more diffuse areas of ammonia to the south-east of these agricultural valleys over arid areas could be due to the transport of polluted air by the prevailing winds in this region over the Takla Makan desert. Very little ammonia is detected in the high altitude areas of the Himalayas and Tian Shan Mountain Range, which are mostly uncultivated. Levels of ammonia over ocean are expected to be extremely low except in the case of transport from polluted areas over land. Observations over land generally have better sensitivity to ammonia in the boundary layer than observations over ocean during the day due to higher thermal contrast with the surface. Bearing this in mind, there are signs of transport eastward out of India over the Bay of Bengal.

The detected total column ammonia in Figs. 10 and 11 is given in apparent mg m^{-2}. Whether or not these values reflect the true column amount depends on the linearity of the ammonia absorption versus abundance, the assumed shape of the profile, and the actual thermal contrast conditions. In the case of ammonia, the vertical distribution is fairly constant with a maximum in the boundary layer which quickly decays with altitude. It is also so weakly absorbing that radiative transfer is usually within the linear regime. These characteristics mean that it is reasonable to produce a conversion factor from the observed BTD to estimated true column amount as in Clarisse et al. (2009). This species is therefore also suitable candidate for producing an estimate of the true abundance using the new method. However, the apparent signal strength is strongly dependent on the thermal contrast between the first atmospheric layers and the surface. The apparent column amounts for daytime ammonia are several times higher than the total column values retrieved by Clarisse et al. (2009) using a full optimal estimation retrieval taking into account the thermal contrast conditions for this scene. Their retrieved values for this region reached 7.5 mg m^{-2} across the Indo-Gangetic Plane for this orbit, whereas the maximum estimated column values for the new filter are above 20 mg m^{-2} in this region. As was confirmed in simulations, the relationship between absorption and abundance is close to to linear for ammonia, which is a weakly absorping and far from saturation, and the higher than expected column amounts can mostly be

AMTD
3, 4531–4569, 2010

attributed to the postive thermal contrast between the surface and lower atmospheric layers for the morning orbit which is not included in the generation of the filter where conditions of no thermal contrast were assumed.

Favorable thermal contrast during the day makes the detection of ammonia easier but does mean that characterising the true amount is more difficult because it depends on a knowledge of the thermal contrast conditions between the surface and the first atmospheric layers. However, the new filter is sufficiently sensitive to detect ammonia at night when the surface temperature is generally similar to the lower atmospheric layers. The results for the nighttime overpass on the 13 May 2008 are shown in Figs. 13 and 14. The 99% confidence threshold for a positive detection identifies a swath of high values in this region, as well as in several regions further north using the new filter, whereas no ammonia is positively identified using this threshold with the three channel filter. The new filter estimates column amounts for NH_3 of up to 6.8 mg m^{-2} for this scene, which is much lower than the estimated column value during the day, and more closely agrees with the values derived by Clarisse et al. (2009) in a full-retrieval. The nighttime spectra correspond better to the assumption of zero thermal contrast used to generate the ammonia filter and so more realistic values can be expected. However, due to the lack of thermal contrast and therefore sensitivity to the boundary layer, it is likely that very low altitude ammonia is missed at night.

3 Conclusions

An extension of the Brightness Temperature Difference method for the detection of trace species was presented and was demonstrated for the detection of sulphur dioxide and ammonia from MetOp IASI. The method allows the construction of many channel filters with a set of linear weights for the detection of the target species and suppression of other unwanted parameters. The method is based on a linear joint retrieval of the target species and brightness temperature offset using the total measurement error variance-covariance to weight the least-squares inversion. The total measurement

AMTD
3, 4531–4569, 2010

error variance-covariance is key to the suppression of unwanted parameters in the detection. This matrix can be constructed either through consideration of appropriate perturbations to the forward model, or by using an appropriate ensemble of measured spectra to construct an estimate of the total measurement error variance-covariance for the background atmosphere. Filters with very good signal to noise characteristics can be produced using these methods which effectively suppress the contribution of unwanted parameters. Very sensitive detections of volcanic sulphur dioxide and ammonia associated with agriculture were possible using the new filters. The technique should be applicable to any spectrometer.

References

Cayla, F., Tournier, B., and Hebert, P.: Performance budgets of IASI options, Tech. rep., Centre National d'Études Spatiales, 1995. 4544, 4550

Clarisse, L., Coheur, P. F., Prata, A. J., Hurtmans, D., Razavi, A., Phulpin, T., Hadji-Lazaro, J., and Clerbaux, C.: Tracking and quantifying volcanic SO_2 with IASI, the September 2007 eruption at Jebel at Tair, Atmos. Chem. Phys., 8, 7723–7734, doi:10.5194/acp-8-7723-2008, 2008. 4534, 4558

Clarisse, L., Clerbaux, C., Dentener, F., Hurtmans, D., and Coheur, P.: Global ammonia distribution derived from infrared satellite observations, Nature Geosci., 2, 479–483, doi:10.1038/ngeo551, http://dx.doi.org/10.1038/ngeo551, 2009. 4535, 4549, 4550, 4551, 4552, 4553

Dudhia, A.: Reference Forward Model (RFM) [Internet], http://www.atm.ox.ac.uk/RFM, 2008. 4544

Food and Agriculture Organization of the United Nations: FAOSTAT landuse database, [Internet], http://faostat.fao.org/site/377/default.aspx#ancor, 2008. 4551

Guffanti, M., Schneider, D., Ewert, J., and Targosz, S.: Impact on aviation operations of volcanic gas and ash clouds from the 2008 eruptions of Okmok and Kasatochi, Alaska, in: AGU Fall Meeting Abstracts, vol. 1, p. 0277, 2008. 4544

Hadji-Lazaro, J., Clerbaux, C., Couvert, P., Chazette, P., and Boonne, C.: Cloud filter for CO

AMTD
3, 4531–4569, 2010

retrieval from IMG infrared spectra using ECMWF temperatures and POLDER cloud data, Geophys. Res. Lett., 28, 2397–2400, 2001. 4550

Karagulian, F., Clarisse, L., Clerbaux, C., Prata, A. J., Hurtmans, D., and Coheur, P. F.: Detection of volcanic SO_2, ash, and H_2SO_4 using the Infrared Atmospheric Sounding Interferometer (IASI), J. Geophys. Res., 115, D00L02, doi:10.1029/2009JD012786, 2010. 4544

OMI Volcanic Emissions Group TOMS: AIRS Volcanic Image Archive, [Internet], http://toms.umbc.edu/, 2010. 4534

OMI/Aura [Internet]: http://earthobservatory.nasa.gov/IOTD/view.php?id=8998, 2010. 4544

Prata, A.: Satellite detection of hazardous volcanic clouds and the risk to global air traffic, Nat. Hazards, 51, 303–324, 2009. 4534

Remedios, J. J., Leigh, R. J., Waterfall, A. M., Moore, D. P., Sembhi, H., Parkes, I., Greenhough, J., Chipperfield, M. P., and Hauglustaine, D.: MIPAS reference atmospheres and comparisons to V4.61/V4.62 MIPAS level 2 geophysical data sets, Atmos. Chem. Phys. Discuss., 7, 9973–10017, doi:10.5194/acpd-7-9973-2007, 2007. 4546, 4548

Rix, M., Valks, P., Hao, N., van Geffen, J., Clerbaux, C., Clarisse, L., and Coheur, P. F.: Satellite Monitoring of Volcanic Sulfur Dioxide Emissions for Early Warning of Volcanic Hazards, IEEE Journal of Selected Topics in Applied Earth Observations and Remote Sensing, 2, 2009. 4534

Rodgers, C. D.: Inverse Methods for Atmospheric Sounding, World Scientific, 2000. 4536

van Geffen, J., Van Roozendael, M., van Gent, J., Valks, P., and Rix, M.: An alert system for volcanic SO2 emissions using satellite measurements, 2009. 4534

von Clarmann, T., Grabowski, U., and Kiefer, M.: On the role of non-random errors in inverse problems in radiative transfer and other applications, J. Quant. Spectros. Radiat. Trans., 71, 39–46, http://www.sciencedirect.com/science/article/B6TVR-43HK0S8-4%2/6d419197d740217d230a53fd4b860e38, 2001. 4538

AMTD
3, 4531–4569, 2010

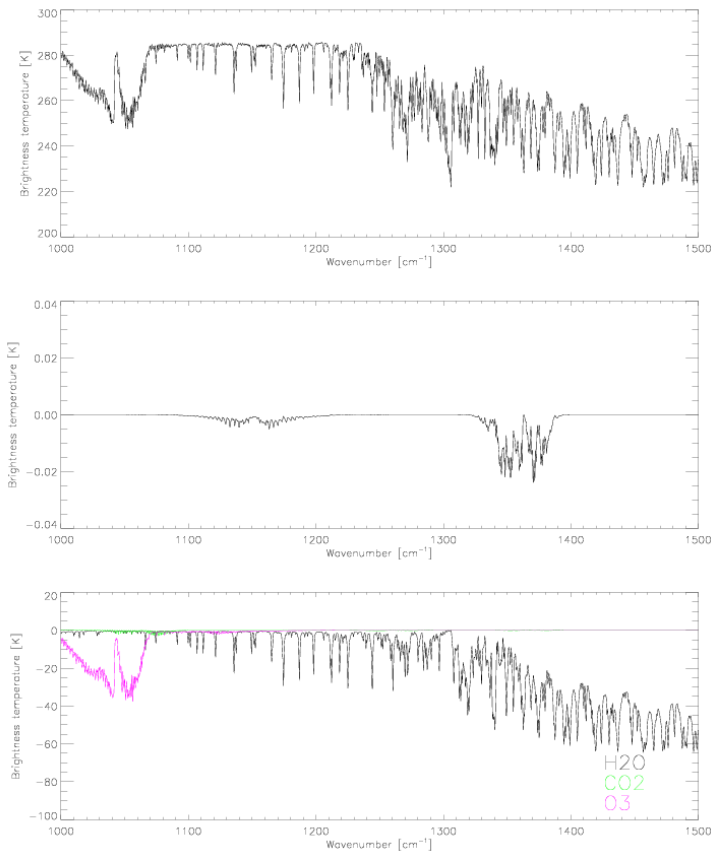

Fig. 1. Simulated spectra in region of SO_2 ν_1 and ν_3 bands. Top panel shows simulated spectrum for standard atmosphere. Middle panel shows contribution of climatological background levels of SO_2. Bottom panel shows contribution of main interfering species (water vapour, CO_2 and ozone).

AMTD
3, 4531–4569, 2010

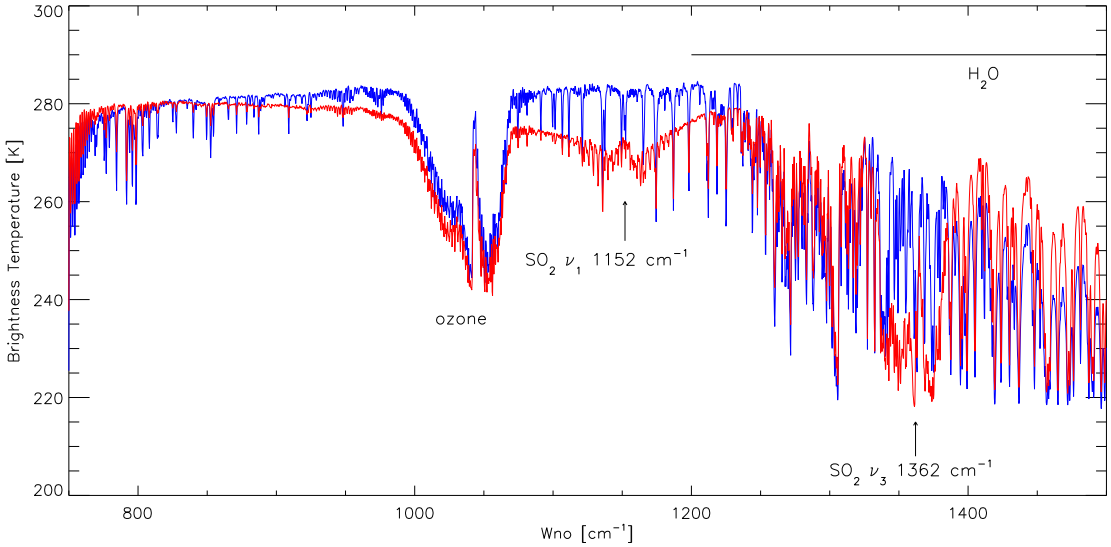

Fig. 2. Blue line shows an IASI spectrum obtained from outside of the Kasatochi volcanic plume on 10 August over ocean and the red line shows an IASI spectrum obtained inside the plume.

AMTD
3, 4531–4569, 2010

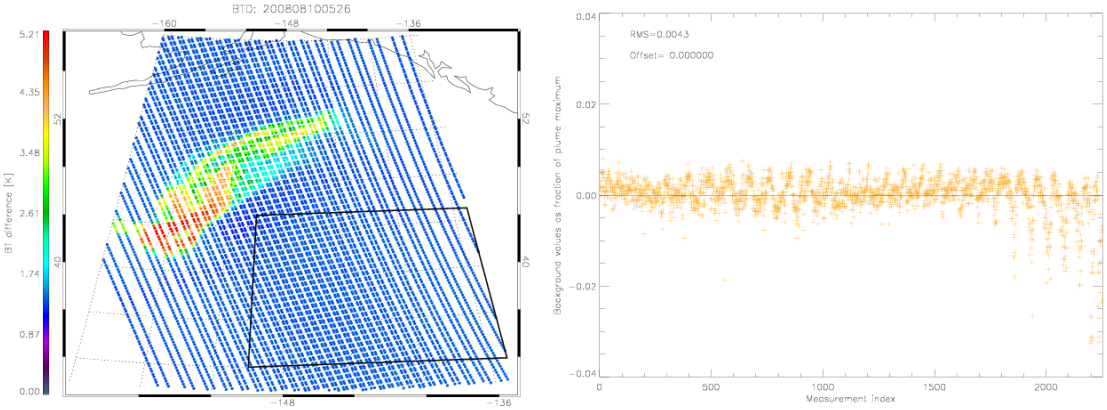

Fig. 3. Detection of SO_2 plume for the Kasatochi eruption for the morning overpass on 10 August 2008 using the four channel BTD by Clarisse et al. (2008) in terms of background channels minus SO_2 sensitive channels. The variation in the spectral background within the box is shown on the right in terms of the fractional variation normalised with respect to the maximum BT value observed inside the plume. Observed RMS of background (excluding values below −0.01) = 0.0033.

AMTD
3, 4531–4569, 2010

Method for the detection of trace species in IASI data

J. C. Walker et al.

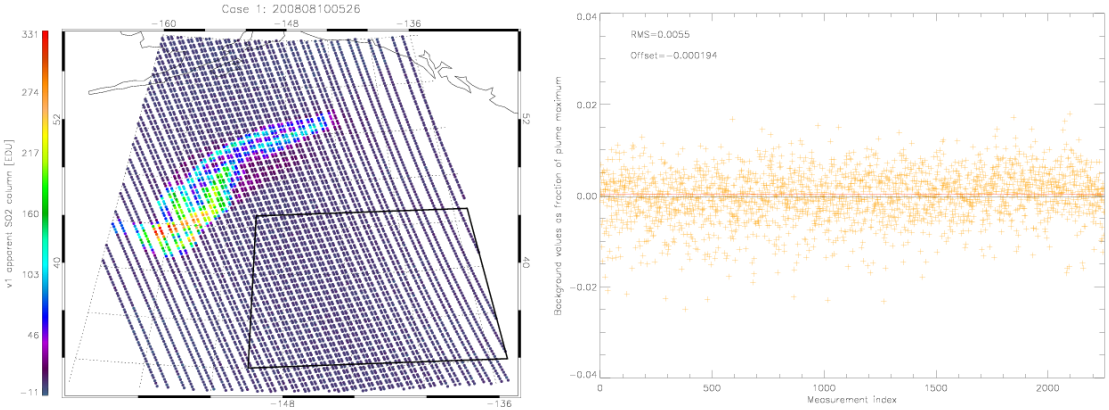

Fig. 4. The plume of SO_2 for the morning overpass on 10 August 2008 using the ν_1 band filter for Cases (1) as described in the text using the modelling approach compute $\mathbf{S}_y^{\text{tot}}$. Fractional variation in the background normalised according to the maximum value within the plume shown in figure on the right for IFOV's inside box. Reported 1σ sensitivity (σ_c) for this filter of 0.0022 (=0.734 EDU). Observed RMS of background = 0.0055.

AMTD
3, 4531–4569, 2010

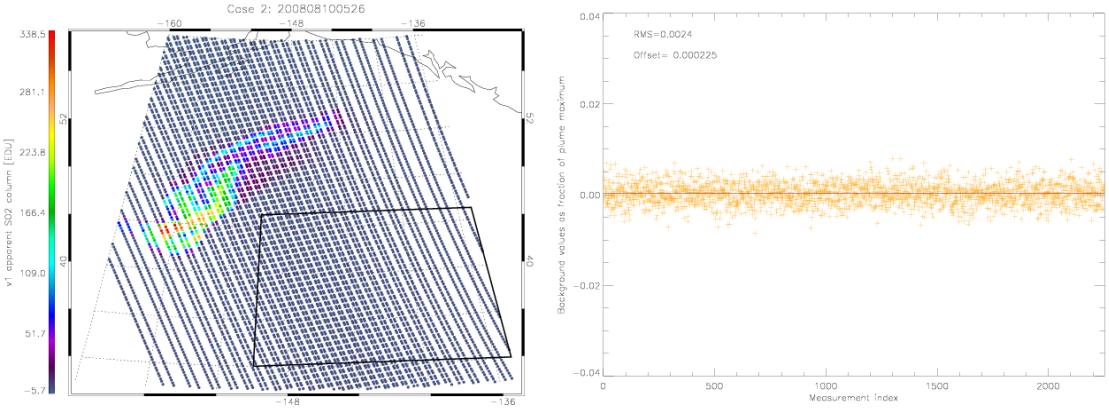

Fig. 5. The plume of SO_2 for the morning overpass on 10 August 2008 using the ν_1 band filter for Cases (2) as described in the text using the ensemble approach compute $\mathbf{S}_y^{\text{tot}}$. Fractional variation in the background normalised according to the maximum value within the plume shown in figure on the right for IFOV's inside box. Reported 1σ sensitivity (σ_c) for this filter of 0.0024 (=0.812 EDU). Observed RMS of background = 0.0024.

AMTD
3, 4531–4569, 2010

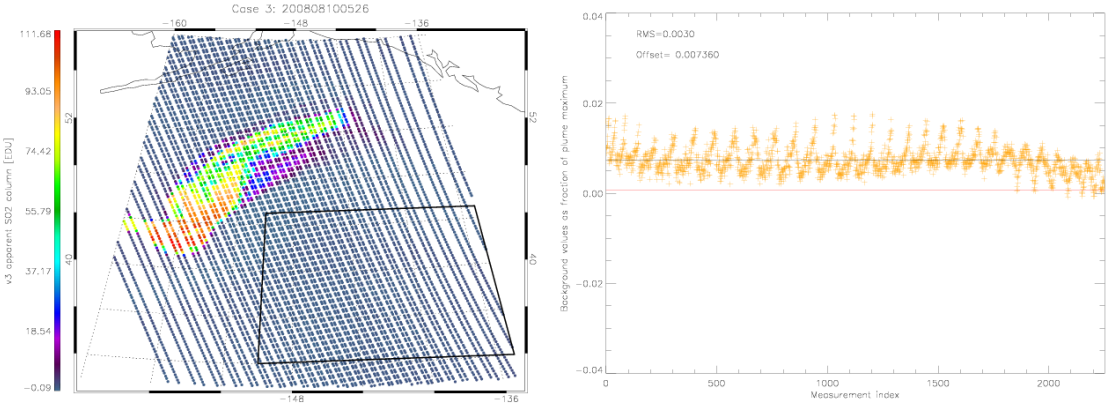

Fig. 6. The plume of SO_2 for the morning overpass on 10 August 2008 using the ν_3 band filter for Case (1) as described in the text using the modelling approach compute $\mathbf{S}_y^{\text{tot}}$. Fractional variation in the background normalised according to the maximum value within the plume shown in figure on the right for IFOV's inside box. Reported 1σ sensitivity (σ_c) for this filter of 0.0013 (=0.122 EDU). Observed RMS of background = 0.0030. Expected climatological value shown as red line. Mean value of background value shown as black line.

AMTD
3, 4531–4569, 2010

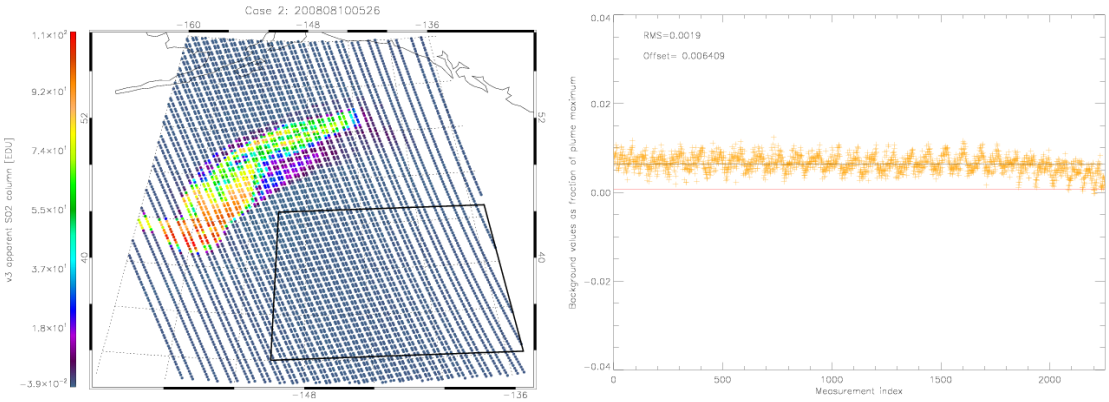

Fig. 7. The plume of SO_2 for the morning overpass on 10 August 2008 using the ν_3 band filter for Case (2) as described in the text using the modelling approach compute $\mathbf{S}_y^{\text{tot}}$. Fractional variation in the background normalised according to the maximum value within the plume shown in figure on the right for IFOV's inside box. Reported 1σ sensitivity (σ_c) for this filter of 0.0012 (=0.126 EDU). Observed RMS of background = 0.0019. Expected climatological value shown as red line. Mean value of background value shown as black line.

AMTD
3, 4531–4569, 2010

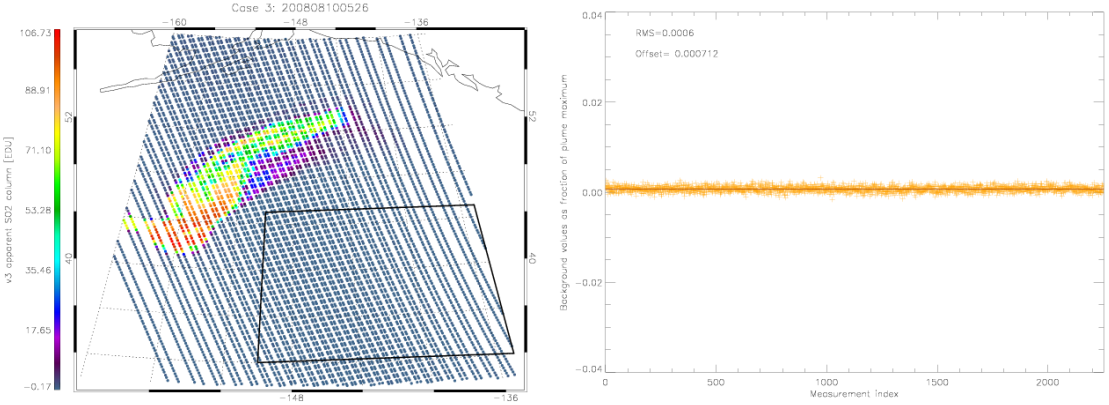

Fig. 8. The plume of SO_2 for the morning overpass on 10 August 2008 using the ν_3 band filter for Cases (3) as described in the text using the ensemble approach compute $\mathbf{S}_y^{\text{tot}}$. Fractional variation in the background normalised according to the maximum value within the plume shown in figure on the right for IFOV's inside box. Reported 1σ sensitivity (σ_c) for this filter of 0.0006 (=0.067 EDU). Observed RMS of background = 0.0006.

AMTD
3, 4531–4569, 2010

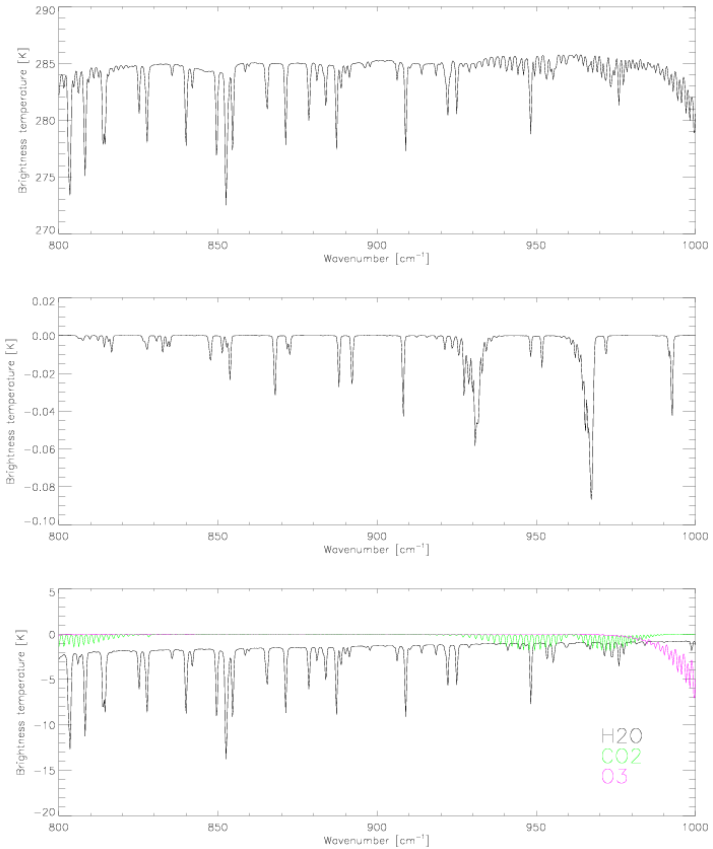

Fig. 9. Simulated spectra in region of ammonia ν_2 band. Top panel shows simulated spectrum for standard atmosphere. Middle panel shows contribution of background levels of ammonia. Bottom panel shows contribution of main interfering species (water vapour, CO_2 and ozone).

AMTD
3, 4531–4569, 2010

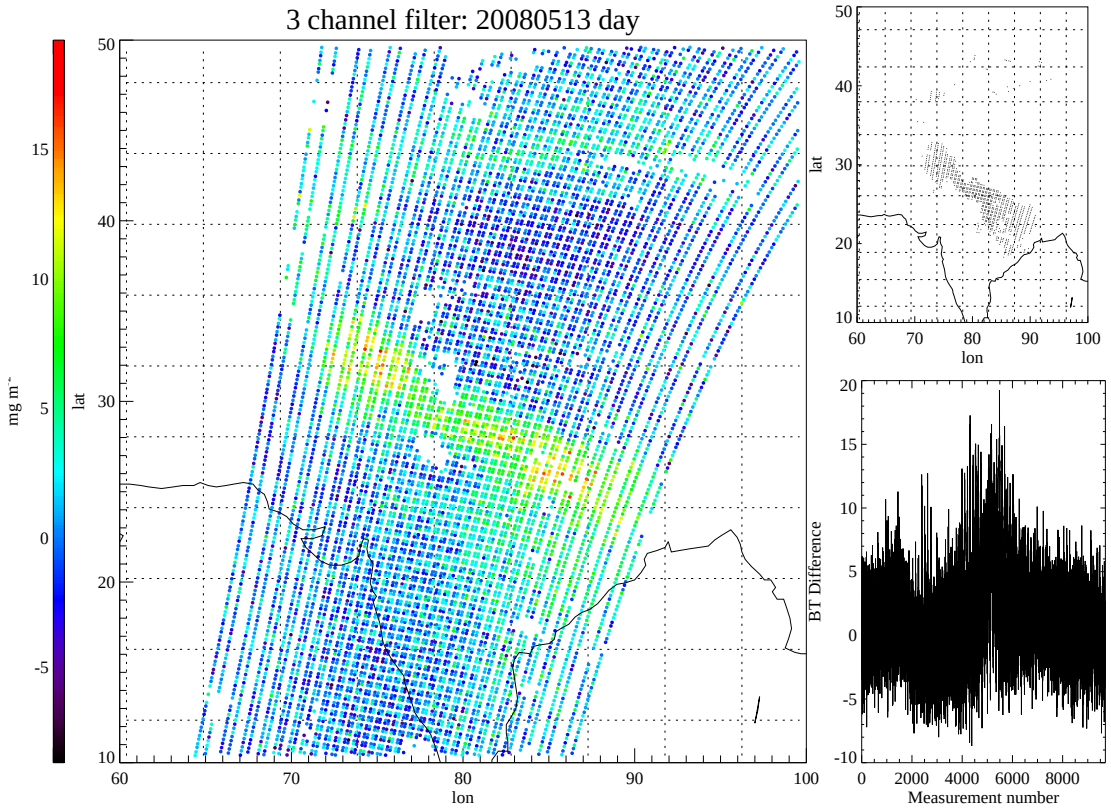

Fig. 10. Ammonia detected across Asia for the morning overpass on 13 May 2008 using the existing three channel filter with estimated total column amounts given in mg m^{-2}. A map of positive detections in the 99% confidence interval are shown in the top-right panel of each figure. The distribution of detected ammonia for each measurement is shown in the bottom-right panel of each figure.

AMTD
3, 4531–4569, 2010

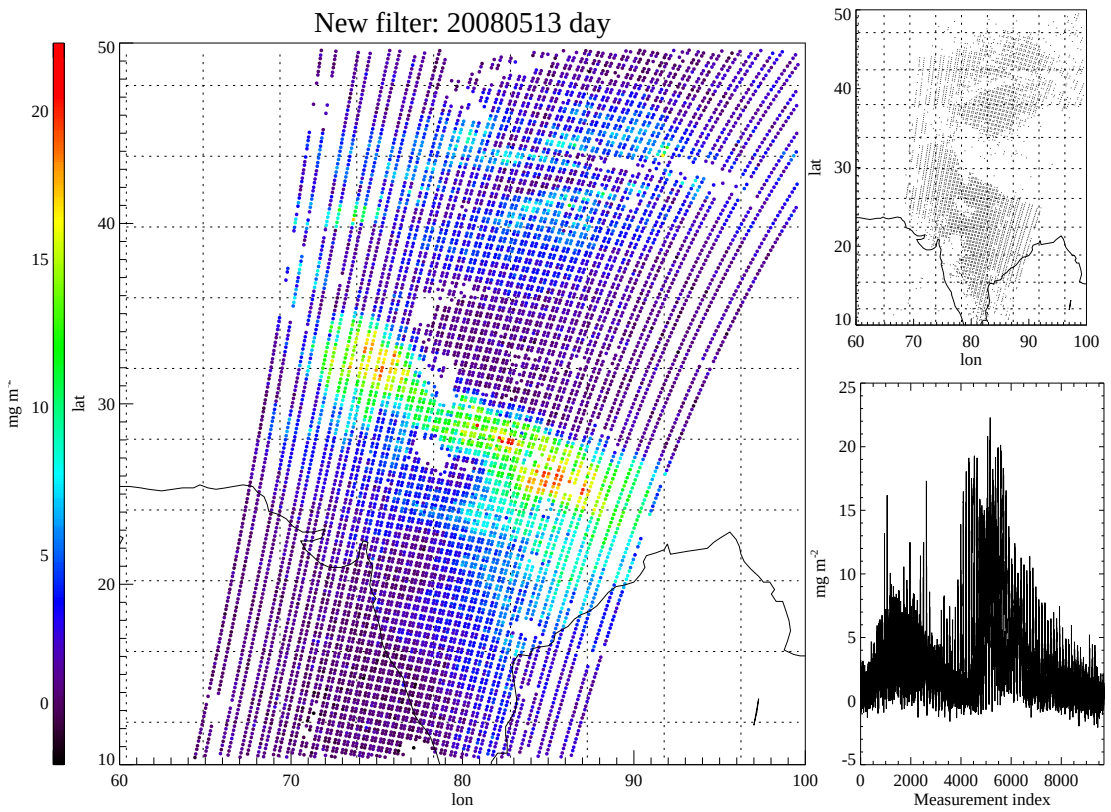

Fig. 11. As in Fig. 10 but using using the new filter for ammonia.

AMTD
3, 4531–4569, 2010

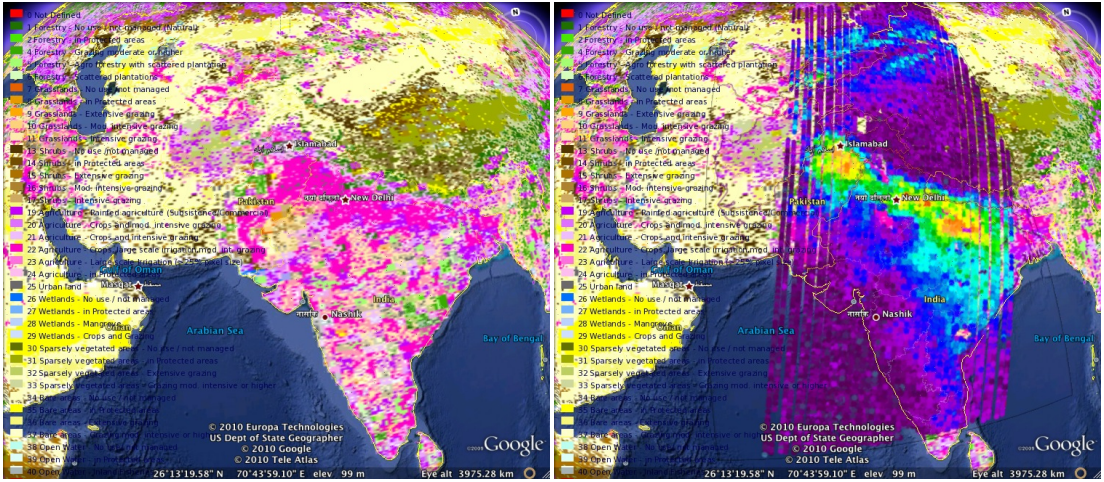

Fig. 12. Ammonia as seen by IASI across Asia for the morning overpass on 13 May 2008 using the new filter. The left panel shows a map of landuse, where pink and purple colours correspond to agriculture, green colours correspond to sparsely vegetated or forested areas, and yellow colours correspond to bare areas. Right panel shows ammonia overlaid onto the landuse map. Individual IASI pixels are larger than true scale.

AMTD
3, 4531–4569, 2010

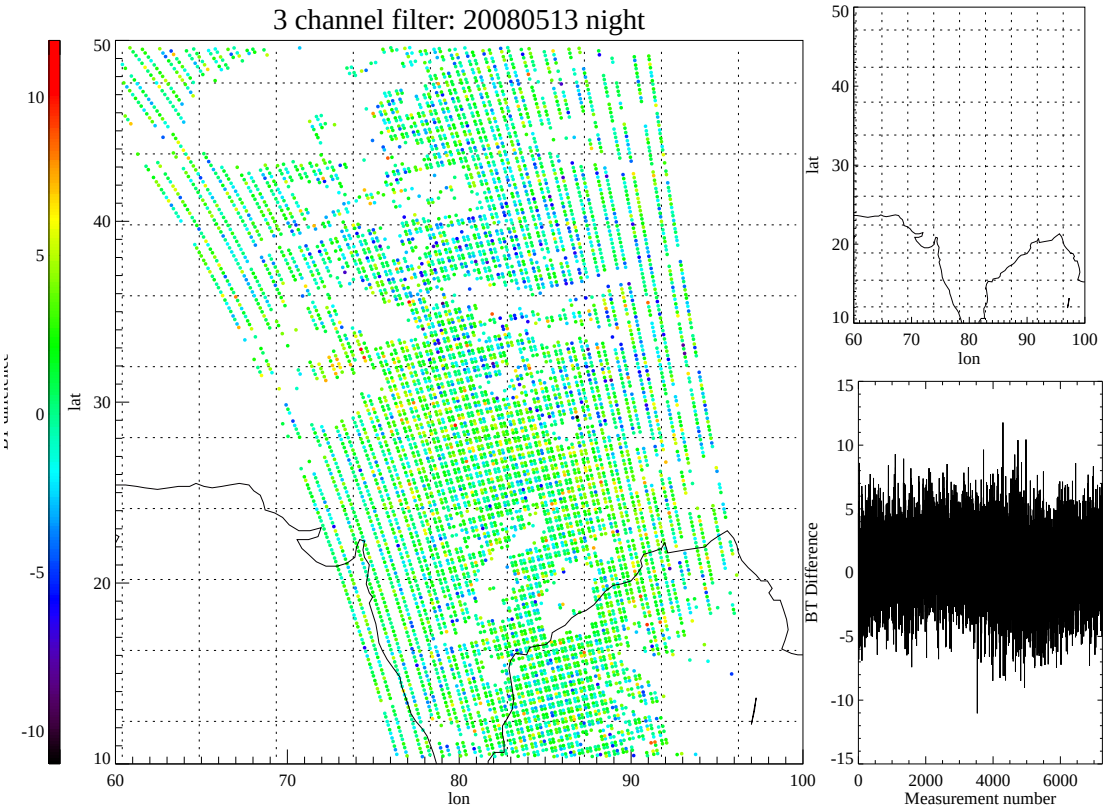

Fig. 13. Ammonia as seen by IASI for the nighttime overpass on 13 May 2008 using the exising three channel filter with estimated total column amounts given in mg m^{-2}. A map of positive detections in the 99% confidence interval are shown in the top-right panel of each figure. The distribution of detected ammonia for each measurement is shown in the bottom-right panel. Cloudy scenes have been removed.

AMTD
3, 4531–4569, 2010

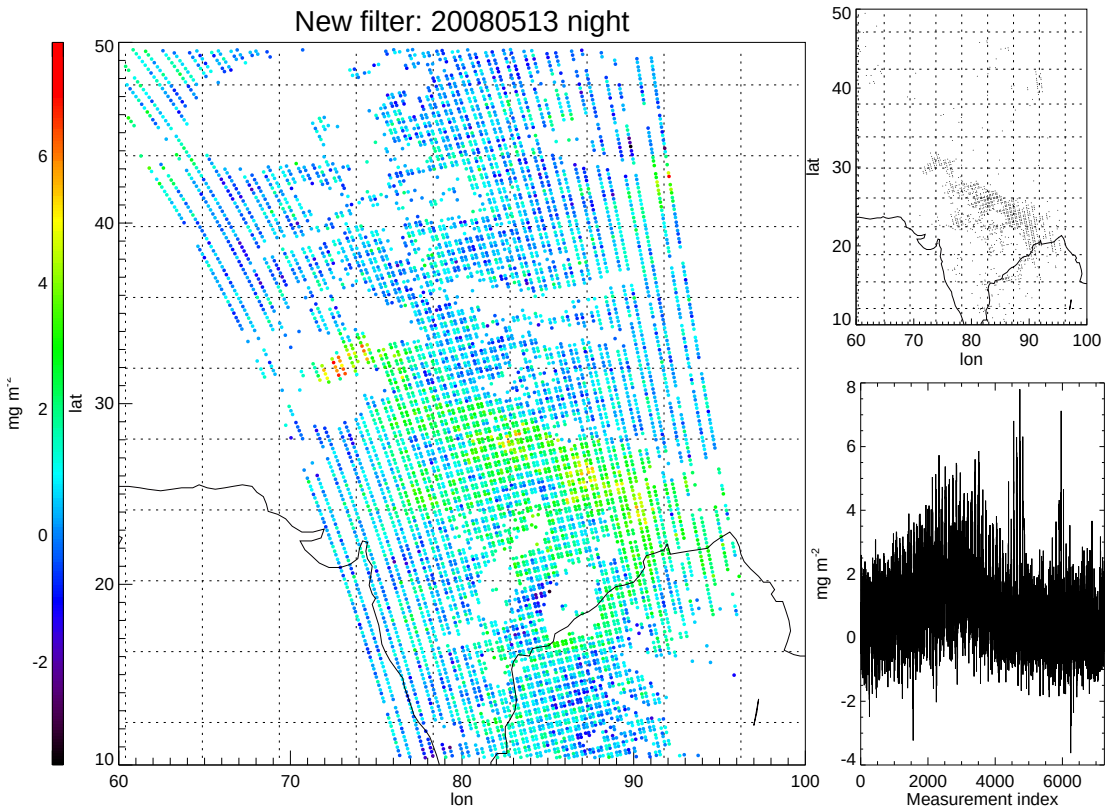

Fig. 14. As in Fig. 13 but using the new ammonia filter.

AMTD
3, 4531–4569, 2010

Method for the detection of trace species in IASI data

J. C. Walker et al.